Plasma Sources Science and Technology

PAPER

Study of temporal dissociation and atomic excitation rates in a flowing N_2 DC discharge and post-discharge

To cite this article: J Levaton *et al* 2022 *Plasma Sources Sci. Technol.* **31** 125010

View the article online for updates and enhancements.

You may also like

- Modelling N_2–O_2 plasmas: volume and surface kinetics
Vasco Guerra, Antonio Tejero-del-Caz, Carlos D Pintassilgo et al.
- Investigation of N(^{4}S) kinetics during the transients of a strongly emissive pulsed ECR plasma using ns-TALIF
E Bisceglia, S Prasanna, K Gazeli et al.
- N_2 dissociation and kinetics of N(^{4}S) atoms in nitrogen DC glow discharge
A V Volynets, D V Lopaev, T V Rakhimova et al.

This content was downloaded from IP address 143.107.135.170 on 06/03/2023 at 20:54

IOP Publishing Plasma Sources Science and Technology
Plasma Sources Sci. Technol. **31** (2022) 125010 (13pp) https://doi.org/10.1088/1361-6595/acacc2

Study of temporal dissociation and atomic excitation rates in a flowing N_2 DC discharge and post-discharge

J Levaton[1,*], A N Klein[1], J Amorim[2] and J H F Severo[3]

[1] Laboratório de Materiais (LABMAT), Departamento de Engenharia Mecânica, Universidade Federal de Santa Catarina, 88040-900 Florianópolis, SC, Brazil
[2] Departamento de Física, Instituto Tecnológico de Aeronáutica, 12228-900 São José dos Campos, SP, Brazil
[3] Laboratório de Física de Plasmas, Instituto de Física, Universidade de São Paulo, 05508-090 São Paulo, SP, Brazil

E-mail: jacques.levaton@gmail.com

Received 9 August 2022, revised 23 November 2022
Accepted for publication 19 December 2022
Published 30 December 2022

Abstract

In this work, we experimentally and theoretically study mechanisms of molecular dissociation and atomic excitation occurring in a flowing nitrogen DC discharge and its post-discharge. A specific discharge experimental condition for the pink afterglow plasma occurrence in the post-discharge tube is analyzed. We employ optical emission spectroscopy (OES) and Langmuir probes to measure the reduced electric field (E/N), electron density (n_e), gas temperature (T_g) and $N_2(X^1\Sigma^+_g)$ vibrational temperature (T_v) in the positive column. OES was also employed in the post-discharge for measurements of relative densities of $N(^4S)$ and $N(^2D)$ atoms in the pink afterglow. Two well-established numerical kinetic models, one for the positive column and another one for the post-discharge, were used to calculate the rates of molecular dissociation and atomic excitation as a function of gas residence time in the positive column and also in the nitrogen post-discharge. We analyzed the role of 13 molecular dissociation mechanisms, and 8 atomic excitation mechanisms in the positive column and pink afterglow. Results demonstrate that the positive column dissociation processes are dominated by the direct electron impact mechanism in the earlier discharge gas residence times and that, for longer times, reactions between electronically excited states and $N_2(X^1\Sigma^+_g, v)$ vibrational states become the dominant dissociation mechanisms. It is also observed that dissociation processes occurring in the pink afterglow present relevant rates as compared to the same processes occurring in the positive column, demonstrating the high effectiveness of such processes in the post-discharge. The $N(^2D)$ and $N(^2P)$ excitation mechanisms are also examined. We observe that molecular dissociation and atomic excitation mechanisms strongly depend on the $N_2(X^1\Sigma^+_g)$ vibrational distribution function of the discharge and post-discharge.

* Author to whom any correspondence should be addressed.

 © 2022 IOP Publishing Ltd

Keywords: nitrogen flowing discharge, nitrogen flowing post-discharge, kinetic modeling, dissociation rates, atoms excitation rates

(Some figures may appear in colour only in the online journal)

1. Introduction

$N(^4S)$ atoms are important for the thermochemical treatments of materials carried out in the post-discharge of pure nitrogen and nitrogen–argon–hydrogen flowing discharges. Ricard *et al* [1] obtained a nitrided γ' layer of 6–10 μm and ε layer of 1 μm in a steel surface nitriding treatment carried out in the post-discharge of 2.45 GHz microwave flowing discharges for the introduction of H_2 gas in the nitrogen discharge in the first initial part (2–3 min) of a 1 h treatment. The layers are produced due to the high density of $N(^4S)$ atoms in the post-discharge. The nitrogen atomic density is also correlated to the growth of the ε layer thickness in the post-discharge surface nitriding of Fe—0.1% C substrate [2]. In addition to the purposes of material treatment, $N(^4S)$ atoms play an important role in the kinetic processes that occur in nitrogen discharges and post-discharges. These atoms are the main source of vibrational deactivation of $N_2(X^1\Sigma^+_g, v)$ states by the vibrational–translational (V–T) exchange reactions [3] between $N_2(X^1\Sigma^+_g, v)$–$N(^4S)$ species, inducing the multi-quantum vibrational deactivation processes [4, 5]. Determination of $N(^4S)$ atomic density is crucial to the materials treatments studies, as well as to the studies on the nitrogen plasmas kinetics mechanisms. The actinometry experimental technique is a useful tool in the atom density estimation in the discharges. Czerwiec *et al* [6], employed actinometry to analyze the $N(^4S)$ atoms production in low-pressure cylindrical inductively coupled plasma (ICP) discharges. They utilized mass spectrometry to validate the data obtained by actinometry. Levaton *et al* [7], obtained the absolute density of $N(^4S)$ atoms in 2.45 GHz surface wave discharges as a function of discharge gas pressure and power, using the actinometry technique, together with the nitrogen post-discharge NO titration method. Volynets *et al* [8], studied the kinetics of $N(^4S)$ atoms in a DC nitrogen glow discharge employing actinometry and a 1D radial self-consistent numerical model.

They presented the nitrogen degree of dissociation in these discharges as a function of the gas pressure parameter.

The role of physical-chemical processes related to the $N(^4S)$ production, or equivalently, the nitrogen molecular dissociation mechanisms in the nitrogen discharges are of primary interest in nitrogen plasmas studies [9–11]. Cacciatore *et al* [9] studied the effects of electron collisions with the $N_2(X^1\Sigma^+_g, v)$ states and pure vibrational mechanisms (PVM) in the nitrogen dissociation processes occurring in a nitrogen DC glow discharge. They developed a state-to-state kinetic numerical model to analyze these dissociation mechanisms as functions of the discharge residence time. Kumar and Ghosh [10], studied the nitrogen dissociation in nitrogen DC flowing discharges by mass spectrometry and a simple collisional-radiative numerical model. The degree of dissociation was fully expressed as a function of the electron density and electron temperature parameters of the discharges. Guerra *et al* [11] obtained the relative dissociation rates and $N(^4S)$ atomic concentrations in nitrogen DC discharges using a self-consistent kinetic numerical model and the experimental technique of electron spin resonance. They could determine the relative contribution in the total molecular dissociation for some kinetic mechanisms, including electron collisions dissociation mechanism and dissociation promoted by collisions of electronically excited states and vibrational excited states, as a function of the gas pressure parameter of the discharges. They showed that the participation of excited molecular state collisions increases with the gas pressure parameter and outweighs the participation of the electron collision dissociation mechanism in the total dissociation rates of the discharges.

The $N(^4S)$ density and molecular dissociation mechanisms were also studied in the nitrogen pink afterglow [12–14]. The pink afterglow is a kind of nitrogen plasma generated in the post-discharge of nitrogen flowing discharges. It has been detected in the afterglow of DC [5, 15, 16], radio frequency (RF) [17], and microwave [18, 19] flowing discharges. The excitation, dissociation, and ionization processes occurring in the pink afterglow plasma of the nitrogen flowing DC discharges are induced by physicochemical mechanisms that depend on $N_2(X^1\Sigma^+_g, v)$ states as reactants [5, 14]. As the vibrational distribution function (VDF) of the $N_2(X^1\Sigma^+_g)$ fundamental electronic state heats with the post-discharge residence time, the intermediate and high vibrational levels of the $N_2(X^1\Sigma^+_g, v)$ states are populated, and these states become the precursors of the reactions responsible for sustaining the plasma in the post-discharge. The interesting feature of the pink afterglow is the fact that this nitrogen plasma is generated in the afterglow region, which is a zone where there is no direct influence of an external electric field. In our recent work [20], we studied the ionization and ion transfer mechanisms occurring in the positive column and pink afterglow plasma of nitrogen flowing DC discharges. We have observed that physical-chemical mechanisms such as the Penning ionization and associative ionization between electronically excited molecules and metastable atoms play a crucial role in the ionization of these plasmas, overcoming the electrons collisions ionization channels at certain discharges gas residence times in the positive column of discharges operating at high values of reduced electric field. Furthermore, we observe that the ionization mechanisms occurring in the pink afterglow exhibit significant ionization rates relative to the ionization rates achieved in the positive column. These intriguing characteristics of the ionization mechanisms of the positive columns and pink afterglow of flowing DC discharges lead us to ask how do the

molecular dissociation and atoms excitation mechanisms in the same plasmas work? In this sense, we will analyze in this work, the dissociation and atoms excitation processes occurring in a positive column and pink afterglow plasma of the flowing nitrogen DC discharges. A specific experimental condition of gas pressure, gas flow rate, and discharge current was chosen in such a way the pink afterglow was generated in the post-discharge tube. The reduced electric field (E/N), electron density (n_e), discharge degree of ionization (n_e/N), and gas temperature (T_g) were measured, and these values are input parameters to the positive column kinetic numerical model that we have developed to study the discharge kinetics. The model calculates the rate constants and the densities of 18 different electronic states of nitrogen species as functions of the discharge gas residence time [21]. The densities of the vibrational states of the electronic fundamental state of the nitrogen molecules are also calculated. We find the dissociation and $N(^2D)$, and $N(^2P)$ excitation rates from the densities and rate constants for the analyzed experimental condition. Another kinetic numerical model has been developed to study nitrogen post-discharge [5, 22] and to calculate the atomic dissociation and excitation rates in a nitrogen-pink afterglow plasma. The absolute rates of dissociation analysis and atoms excitation in both the positive column and pink afterglow allow us to compare the effectiveness of such mechanisms in two different nitrogen plasmas, one under the direct influence of an external electric field (positive column), and the other without it (pink afterglow). This is the first time that a considerable group of molecular dissociation and atoms excitation processes is studied as functions of the discharge and post-discharge gas residence times. In addition, this is the first time that a comparison of the effectiveness of dissociation and atoms excitation mechanisms is analyzed in flowing nitrogen DC discharges and post-discharges.

2. Experimental set-up and results

The experimental set-up utilized in the present work is the same as those utilized in earlier studies where the experimental schematic was presented in detail [14, 23]. The positive column and pink afterglow were generated in a flow of high purity nitrogen gas (99.999%), in discharge and post-discharge tubes made of Pyrex glass, with 1.4 cm i.d., connected by a Wood trap arrangement. The positive column electric field was maintained between two side-armed electrodes located 20 cm apart in the discharge tube by a high voltage direct current source. Double Langmuir probes located 10 cm apart were inserted in the middle of the discharge tube for positive column voltage drop measurements. The discharge electric current was measured by an amperemeter connected to the discharge circuit. From the voltage drop, discharge current, and gas pressure measured by a Baratron gauge (MKS 722 A), we could determine the E/N and n_e [21] values of the positive column. The N_2 gas flow was controlled by a flow meter (MKS 247 C). The low pressure was maintained by a mechanical vacuum pump of 25 $m^3\ h^{-1}$ (E1M18 Edwards). The discharge and post-discharge emissions were measured by a monochromator (Jobin-Yvon, THR-1000) with a 1800 g mm^{-1} grating connected to a photomultiplier tube (Hamamatsu, R928). An optical fiber was used to collect the light from the end of the positive column and along the post-discharge tube. The discharge was carried out with the following experimental conditions: gas flow rate $Q = 0.5$ Sl m^{-1}, gas pressure $p = 500$ Pa, and discharge current $I = 30$ mA. The experimental parameters of the discharge are specified in table 1 presented below. The electron density was calculated from a relationship between the experimental electron's current density and drift velocity [21]. The $N_2(X^1\Sigma^+_g)$ vibrational temperature was measured at the end of the positive column by optical emission spectroscopy (OES). We utilized the transitions of the second positive system of nitrogen molecules [24] in the range of 360–385 nm. The method used to estimate the vibrational temperature from OES in nitrogen glow discharges is detailed and discussed in [25]. The gas temperature was also measured by OES at the end of the positive column. We used the rotational transitions of the first positive system of nitrogen molecules [24] in the range of 760–780 nm [26]. The discharge gas residence time was calculated from a relationship between the inter-electrode distance and gas velocity [20]. The reduced electric field was calculated from the measured electric field at the Langmuir double probes and the Avogadro number of particles calculated for the measured gas temperature (T_g) and pressure. The discharge degree of ionization was obtained from the measured electron density and the estimated number of particles.

Table 1. Experimental discharge parameters: electron density (n_e), $N_2(X^1\Sigma^+_g)$ vibrational temperature (T_v), gas temperature (T_g), gas residence time (τ), reduced electric field (E/N), and degree of ionization (n_e/N).

n_e ($\times 10^{10}$ cm^{-3})	T_v (K)	T_g (K)	τ (ms)	E/N (Td)	n_e/N
5.66 ± 0.15	5100 ± 800	470 ± 50	10.6 ± 2.0	25 ± 3	7.3×10^{-7}

We should note that we used a rotary oil pump in the experiment and that this kind of device can cause the effect of back flow, which can contaminate the post-discharge tube with carbon impurities. Evidence of contamination is given by emissions of CN bands. We did not note contamination of the system. We monitored the CN(0,0) and CN(1,1) bands and did not find emissions from these bands. We followed a cleaning procedure for the system, maintaining the discharge with a mixture of Ar 10%–90% N_2 at a high discharge current value for 2 h before starting the measurements in the pure nitrogen discharge and post-discharge. We also monitored the N_2+(B)(0,0) band intensity that increased considerably after 30 min from the moment we switched on the discharge. The emissions of the N_2+(B)(0,0) band stabilized after this initial time. We got a strong pink afterglow phenomenon after the cleaning procedure. It should be noted that pink afterglow is not formed if contamination is important in the discharges.

3. Modeling results and discussion

The experimental data determined in the experimental section is used as input parameters to the positive column and post-discharge kinetic numerical models employed for the analysis of the dissociation and atom excitation rates. The discharge kinetic numerical model assumes a state-to-state approach where the electron energy distribution function (EEDF) is calculated for the *E*/*N*, n_e, T_g, and $\left(\frac{n_e}{N}\right)$ parameters and the electron collisions excitation, dissociation, and ionization rate constants are obtained from the integration of the reactions cross-sections, electron energy, and EEDF on the energy axis [21]. Once the rate constants have been determined, the model calculates the relaxation of the vibrational master equation (VME) for the $N_2(X^1\Sigma^+{}_g, v)$ states coupled to the rate balance equations for 17 different species of nitrogen. The model furnishes the densities of these species as functions of the discharge gas residence time. The species considered are: $N_2(X^1\Sigma^+{}_g, 0 \leqslant v \leqslant 45)$, $N_2(A^3\Sigma^+{}_u)$, $N_2(B^3\Pi_g)$, $N_2(a^1\Pi_g)$, $N_2(a'^1\Sigma^-{}_u)$, $N_2(w^1\Delta_u)$, $N_2(a''^1\Sigma^+{}_g)$, $N_2(W^3\Delta_u)$, $N_2(E^3\Sigma^+{}_g)$, $N_2(C^3\Pi_u)$, $N_2^+(X^2\Sigma^+{}_g)$, $N_2^+(B^2\Sigma^+{}_u)$, N^+, N_3^+, N_4^+, $N(^4S)$, $N(^2D)$, and $N(^2P)$. The integration in time of the mentioned equations is done in the MATLAB environment, with an ordinary differential equation solver library specially designed to solve Stiff problems [27]. A detailed discussion on the integration method itself is presented in [28]. In addition to the VME which accounts for electron–vibrational (e–V), vibrational–vibrational (V–V), and vibrational–translational (V–T) processes [3], the model accounts for 115 physical-chemical processes among neutral and excited molecular states, atoms, and ions [21]. This kinetic numerical model has been used to study the positive column atoms and molecules densities [21, 29], and ionization and ion transfer processes [20, 30].

The kinetic numerical model for the post-discharge has the same structure as the kinetic numerical model for discharge, i.e. it calculates the VME relaxation coupled to the rate balance equations for the species by the integration in time of these equations [5]. The species considered in this model are: $N_2(X^1\Sigma^+{}_g, 0 \leqslant v \leqslant 45)$, $N_2(A^3\Sigma^+{}_u)$, $N_2(B^3\Pi_g)$, $N_2(a^1\Pi_g)$, $N_2(a'^1\Sigma^-{}_u)$, $N_2(a''^1\Sigma^+{}_g)$, $N_2(C^3\Pi_u)$, $N_2^+(X^2\Sigma^+{}_g)$, $N_2^+(B^2\Sigma^+{}_u)$, N^+, N_3^+, N_4^+, $N(^4S)$, $N(^2D)$, and $N(^2P)$. We consider 66 physical-chemical processes between the neutral and excited molecules, atoms, and ions [22]. The number of processes considered in the post-discharge kinetic model is less than the number of processes in the discharge model since the processes of excitation, dissociation, and ionization by electron collision are not considered due to the low average energy of the electrons in the post-discharge region [5]. The post-discharge model requires as input parameters the densities of the considered species at the end of the discharge. The initial $N_2(X^1\Sigma^+{}_g)$ VDF is assumed as a Boltzmann distribution with the measured vibrational temperature at the end of the positive column [5, 14, 22, 23]. Here, in contrast to our earlier works on the nitrogen post-discharge [5, 14, 22, 23] where we took the initial molecular and atomic densities for the modeling from literature, we consider them as the values calculated at the end of the positive column by the discharge kinetic model. The post-discharge model furnishes the densities of species as functions of the post-discharge gas residence time.

In the present work we considered in the discharge and post-discharge different rate constants for some kinetic processes with respect to former works [21, 22]. The first rate constant concerns the associative ionization process:

$$N\left(^2P\right) + N\left(^2P\right) \rightarrow N_2{}^+(X^2\Sigma^+{}_g) + e, \qquad (1)$$

where we use the rate constant proposed in the work of Popov [31] instead of the rate constant proposed by Matveyev and Silakov [32]. This was done taking into account the fact that the recalculation of the rate constant of reaction (1) through the constant of the reverse process (dissociative recombination) as done in [32] is not correct, since the direct and reverse processes almost certainly go through different auto-ionization electronic states. The second process for which we considered a new rate constant is the reaction:

$$N\left(^2P\right) + N_2(X^1\Sigma_g{}^+) \rightarrow N\left(^4S\right) + N_2(X^1\Sigma_g{}^+). \qquad (2)$$

We use the rate constant proposed by Salmon *et al* [33] since the rate constant used in former works taken from the work of Lin and Kaufman [34] seems to be overestimated. Finally, we added in the kinetics the dissociation process [35]:

$$e + N_2(X^1\Sigma_g{}^+) \rightarrow e + N\left(^4S\right) + N\left(^2D\right). \qquad (3)$$

As we briefly described the structure of the kinetic numerical models, we can now analyze the densities of the atoms in the positive column and pink afterglow plasma. These densities were calculated as functions of the discharge and post-discharge gas residence times for the experimental condition whose parameters are expressed in table 1. In figure 1, we present the $N(^4S)$, $N(^2D)$, and $N(^2P)$ calculated densities in the positive column. The vertical dashed line indicates the residence time corresponding to the end of the positive column in our experiment. Focusing on the $N(^4S)$ density profile, we find that its density grows with time presenting three different slopes. The first one, with the smallest rate of growth, initiates at $t = 10^{-7}$ s, and extends up to $t \sim 6$ ms. The second indicates an abrupt increase in the rate of the density growth, and the third initiating at $t \sim 20$ ms indicates a reduced rate of growth compared to the second. The $N(^2D)$, and $N(^2P)$ density profiles almost follow the trend of the $N(^4S)$ density profile, presenting a decreasing behavior at times ranging from $\sim 3 \times 10^{-5}$ s to ~ 3 ms. The $N(^4S)$ density at the end of the positive column is 6.5×10^{13} cm^{-3}, and the $N(^2D)$, and $N(^2P)$ densities are 6.8×10^{12} cm^{-3} and 2.2×10^{11} cm^{-3}, respectively. This $N(^4S)$ density corresponds to a discharge degree of dissociation of 0.09%. We can compare this degree of dissociation with one obtained in a previous work with a different set-up for the nitrogen DC discharge [29]. In that work, the discharge tube radius had 0.3 cm i.d., $E/N = 94$ Td, $n_e = 1.3 \times 10^{11}$ cm^{-3} and gas pressure of 230 Pa. We found a discharge degree of dissociation of 0.4% at the end of the positive column. If we consider the *E*/*N* and n_e of the present work (see table 1), it should be expected that our discharge degree of dissociation

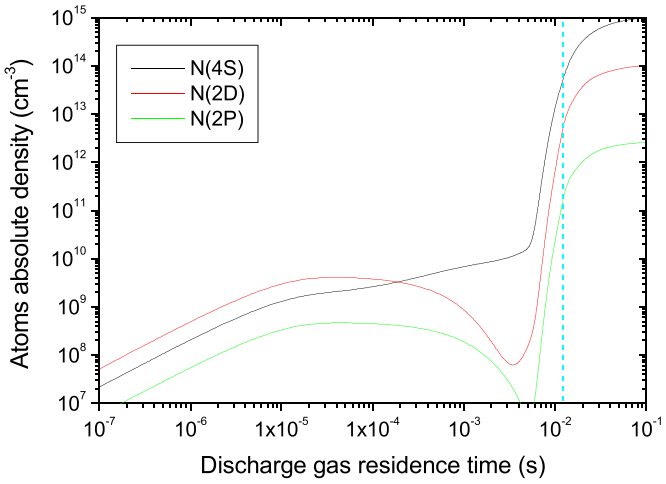

Figure 1. Calculated atomic densities in the positive column as functions of the discharge gas residence time. The N(^{4}S) density (black line), N(^{2}D) (red line), and N(^{2}P) (green line).

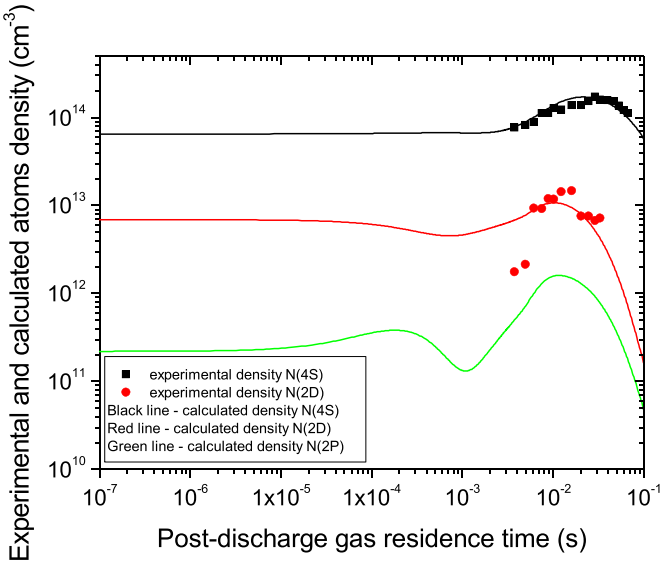

Figure 2. Experimental and calculated atom densities in the post-discharge as functions of the post-discharge gas residence time where the solid lines are the calculated values. The experimental points are the measured densities obtained from OES [36, 37]. The N(^{4}S) density (black line, square symbols), the N(^{2}D) density (red line, circle symbols), and the N(^{2}P) density (green line).

would be inferior to that found in the previous work. The behavior of the atom density profiles will be understood with the analysis of the dissociation and atom excitation rates.

In figure 2, we present the N(^{4}S), N(^{2}D), and N(^{2}P) atomic densities in the post-discharge. The densities are presented as functions of the post-discharge gas residence time. The solid lines are the densities calculated with the post-discharge kinetic numerical model. The initial atomic densities at $t \sim 10^{-7}$ s are those calculated with the discharge kinetic numerical model at the end of the positive column. The experimental points are the N(^{4}S), and N(^{2}D) relative densities obtained by OES from emissions of the first and second positive systems. The methods for measuring the atom's relative densities are discussed in detail in [36, 37]. The error in the experimental densities is approximately 13%.

We note that the calculated atomic densities present the typical behavior of the nitrogen species density profiles in the pink afterglow generated by nitrogen flowing DC discharges [5, 14, 22, 23], that is, a local generation of neutral and excited atoms and excited molecules at post-discharge residence times ranging from ∼1 to ∼20 ms. The same behavior of species densities is found in the pink afterglow of RF discharges [17], and microwave discharges [19]. Eslami and Sadeghi [38], measured the N(^{2}P) absolute density in the pink afterglow of a microwave nitrogen flowing discharge. Their density profile is in good agreement with our N(^{2}P) calculated density profile (see solid green line in figure 2). Their maximum density was $\sim 8 \times 10^{11}$ cm^{-3} at the pink afterglow maximum and our calculated density is $\sim 10^{12}$ cm^{-3} (see solid green line at $t \sim 10$ ms, in figure 2). Popov [31] demonstrated that N(^{2}P) atoms play an important role in the ionization process of the pink afterglow of flowing nitrogen microwave discharges. In his work, he assumed the N(^{2}P) density profile obtained by Eslami and Sadeghi [38] as input and obtained the electron density profile in the post-discharge due to the associative ionization channel via reaction (1). The electron density profile was completely described by this ionization process. Our measured N(^{4}S), and N(^{2}D) relative densities were normalized by the calculated N(^{4}S) density at the pink afterglow maximum (solid black line at $t \sim 20$ ms, in figure 2). We find a good agreement between the experimental and calculated densities concerning the density values and the residence time corresponding to the maximum values. The behavior of the atom density profiles will be understood with the analysis of the dissociation and atom excitation rates in the post-discharge.

We begin our analysis by the consideration of the dissociation rates in the positive column and post-discharge. Among the 115 physical-chemical processes studied in the discharge [21] and the 66 physical-chemical processes studied in the post-discharge [22], the reaction mechanisms leading to the dissociation of molecules are listed in table 2. We take into account the dissociation mechanisms of electron collisions (reactions D1–D7), dissociation promoted by collisions of electronically excited states (reaction D8), dissociation by collisions of electronically excited states and vibrational excited states (reactions D9–D10), dissociation by collisions of vibrational excited states (reaction D11), and dissociation by V–V exchange reactions (reaction D12), and inverse V–T exchange reactions (reaction D13). The reactions occurring in the positive column are reactions D1–D13, and the reactions occurring in the post-discharge are reactions D8–D13 due to the low mean electron energy in the post-discharge [5].

The dissociation rates are defined as the product of the reactants concentrations and rate constant of the dissociation reactions shown in table 2. We calculated the dissociation rates of reactions D1–D13 in the positive column for our experimental condition. In figure 3, we present the dissociation rates concerning the reactions of electrons collisions with neutral and excited molecular states, or reactions D1–D7. It can be

Table 2. Physical-chemical mechanisms leading to molecular dissociation in the positive column and post-discharge.

Process: dissociation mechanisms		k ($cm^3\ s^{-1}$)	References
D1	$e + N_2(X^1\Sigma_g{}^+, v = 0) \rightarrow e + N(^4S) + N(^4S)$	$f\left(\frac{E}{N}, T_g, n_e, p\right)$	[39]
D2	$e + N_2(A^3\Sigma^+{}_u) \rightarrow e + N(^4S) + N(^4S)$	$f\left(\frac{E}{N}, T_g, n_e, p\right)$	[40]
D3	$e + N_2(B^3\Pi_g) \rightarrow e + N(^4S) + N(^4S)$	$f\left(\frac{E}{N}, T_g, n_e, p\right)$	[40]
D4	$e + N_2(a'^1\Sigma^-{}_u) \rightarrow e + N(^4S) + N(^4S)$	$f\left(\frac{E}{N}, T_g, n_e, p\right)$	[40]
D5	$e + N_2(a^1\Pi_g) \rightarrow e + N(^4S) + N(^4S)$	$f\left(\frac{E}{N}, T_g, n_e, p\right)$	[40]
D6	$e + N_2(C^3\Pi_u) \rightarrow e + N(^4S) + N(^4S)$	$f\left(\frac{E}{N}, T_g, n_e, p\right)$	[40]
D7	$e + N_2(E^3\Sigma^+{}_g) \rightarrow e + N(^4S) + N(^4S)$	$f\left(\frac{E}{N}, T_g, n_e, p\right)$	[40]
D8	$N_2(A^3\Sigma^+{}_u) + N_2(A^3\Sigma^+{}_u) \rightarrow N(^4S) + N(^4S) + N_2(X^1\Sigma_g{}^+, v = 0)$	3×10^{-11}	[41]
D9	$N_2(A^3\Sigma^+{}_u) + N_2(X^1\Sigma_g{}^+, v > 13) \rightarrow N(^4S) + N(^4S) + N_2(X^1\Sigma_g{}^+, v = 0)$	$4.5 \times 10^{-11} e^{\frac{-1765}{T}}$	[11]
D10	$N_2(a'^1\Sigma^-{}_u) + N_2(X^1\Sigma_g{}^+, v > 4) \rightarrow N(^4S) + N(^4S) + N_2(X^1\Sigma_g{}^+, v = 0)$	5×10^{-12}	[14]
D11	$2 \times N_2(X^1\Sigma_g{}^+, v > 18) \rightarrow N(^4S) + N(^4S) + N_2(X^1\Sigma_g{}^+, v = 0)$	3.5×10^{-15}	[11]
D12	$N_2(X^1\Sigma^+{}_g, v = 45) + N_2(X^1\Sigma^+{}_g, w) \rightarrow N(^4S) + N(^4S) + N_2(X^1\Sigma^+{}_g, w - 1)$	$Q_{w,w-1}{}^{v,46}$ (T)	[5, 21]
D13	$N_2(X^1\Sigma^+{}_g, v = 45) + N_2(X^1\Sigma^+{}_g) \rightarrow N(^4S) + N(^4S) + N_2(X^1\Sigma^+{}_g)$	$P_{45,46}$ (T)	[5, 21]

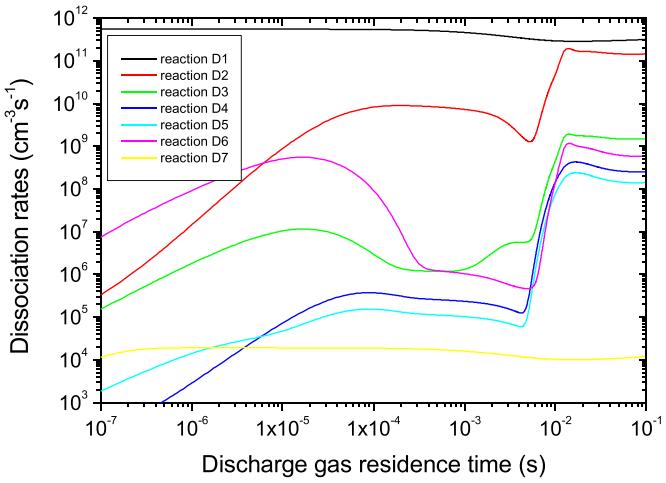

Figure 3. The dissociation rates of electron collision processes in the positive column (reactions D1–D7 in table 2). The curves representing the dissociation rates for each specific reaction are defined in the figure legend.

seen that electron collisions with the nitrogen molecules in the fundamental state (reaction D1) represent the main dissociation mechanism among those involving electron collisional processes. We can also observe that contributions of electronically excited states are less effective, being the collisions of electrons with the first electronic excited state $N_2(A^3\Sigma^+{}_u)$ (reaction D2) significant at times longer than 10 ms as compared to reaction D1. The contribution of higher molecular excited states is too low to cause any significant contribution to the dissociation phenomenon in the positive column. By the consideration of these dissociation rates profiles, we cannot explain the abrupt increase of the $N(^4S)$ density at discharge residence times of the order of 6 ms (see black line in figure 1). In this sense, we will analyze the remaining dissociation processes.

The dissociation rates of reactions concerning the collisions of excited molecules are presented in figure 4. We present the rates of reactions D8–D11, and additionally the rates of reaction D1 in table 2. We can compare the effectiveness of the electron collision dominant dissociation process (reaction D1—see figure 3), and the excited molecules collision dissociation processes. It is observed that reaction D1 is the dominant dissociation channel at residence times from 10^{-7} s to ~2 ms. From 2 ms to 0.1 s the collisions of molecular excited states become the dominant dissociation processes. The dissociation rates of these mechanisms at the maximum of dissociation ($t \sim 15$ ms) are more than four orders of magnitude superior to the dissociation rates of electron collisions with the ground state molecules (reaction D1). The order of the collisional dissociation processes between excited molecules is as follows: reactions D10, D11, D9, and D8. Reaction D10 was proposed to explain the local dissociation process occurring in the pink afterglow of the flowing nitrogen DC discharge [5, 14]. Reactions D11 and D9 were proposed [11] to explain the dissociation processes in the nitrogen DC glow discharge for certain working gas pressures.

We can now correlate the dissociation rate profiles behavior with the $N(^4S)$ density profile behavior (see black line in figure 1). As discussed, the growth of the $N(^4S)$ density presents different slopes. We can associate the first slope from 10^{-7} s to ~6 ms with the dominant dissociation rates from reaction D1, which extends from 10^{-7} s to ~2 ms (see figure 4). The following abrupt increase in $N(^4S)$ density (see figure 1) from $t \sim 6$ ms can be directly associated with the increase in dissociation rates of collisions among excited molecules, mainly by reactions D10, D11, and D9. It is observed that after the fast growth of these dissociation rates, they form a kind of plateau (see figure 4 for $t > 15$ ms). This dissociation rates' behavior explains the slower rate of growth of the $N(^4S)$ atoms density at longer discharge residence times (see figure 1, black line at $t > 20$ ms). The important role of excited molecule collisions in the dissociation phenomenon was demonstrated by Guerra *et al* [11] due to increase in the gas pressure of the studied nitrogen glow discharges. We must take into account that the increase in

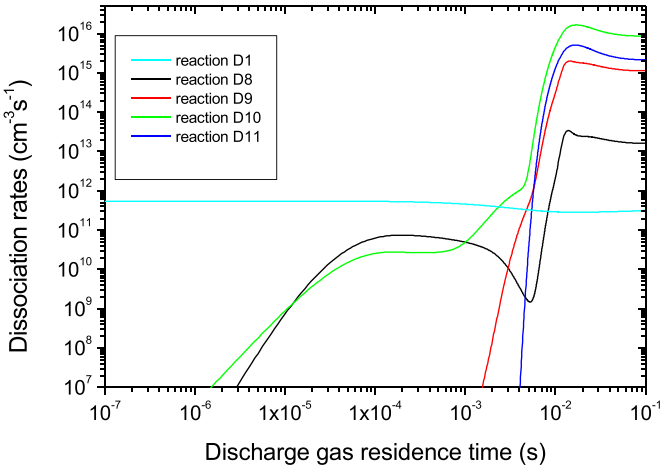

Figure 4. Dissociation rates of electron collisions with the ground state nitrogen molecules process in the positive column (reaction D1 in table 2). Dissociation rates of excited molecules collision processes (reactions D8–D11 in table 2). The curves representing the dissociation rates for each specific reaction are defined in the figure legend.

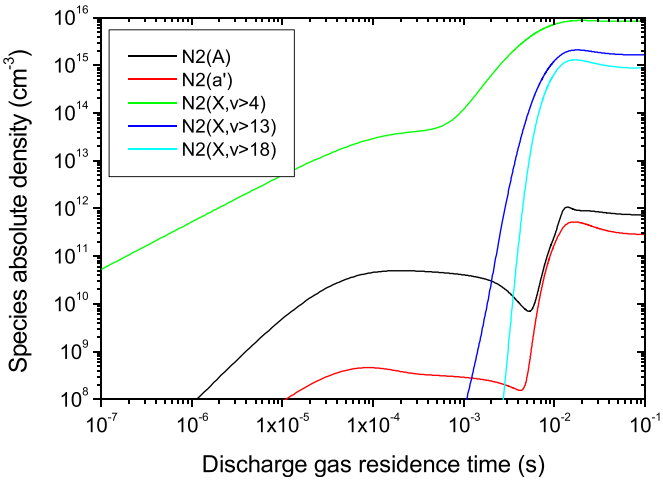

Figure 5. Densities of electronically excited states and $N_2(X^1\Sigma^+{}_g)$ vibrational states as functions of the discharge residence time in the positive column.

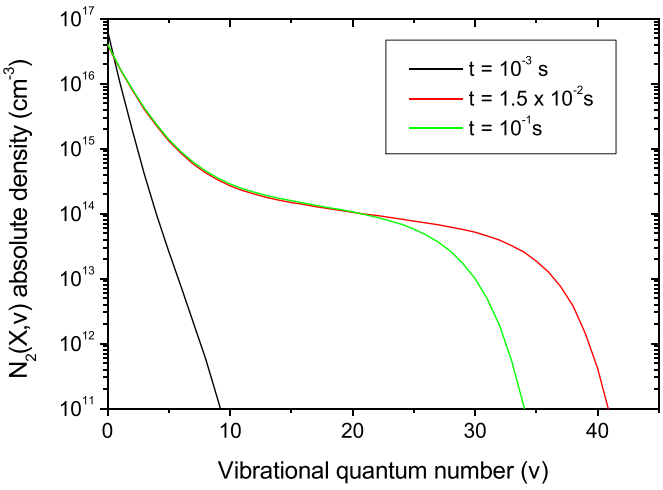

Figure 6. The $N_2(X^1\Sigma^+{}_g)$ VDF in the positive column for residence times of 1, 15, and 100 ms.

the discharge gas pressure results in an increase in the gas residence time [20]. However, they did not consider the occurrence of reaction D10 in their study. Our results evidence the dominant role of electron collisions with the ground state molecule dissociation mechanism (reaction D1) at earlier positive column residence times and the dominant role of reaction D10 at longer discharge residence times. In order to clarify the behavior of the dissociation rates from the collisions of excited molecules, we present in figure 5 the reactants absolute densities of such reactions as functions of the discharge residence time. The first remarkable feature in the densities temporal profiles is the abrupt increase of the vibrational states densities. The $N_2(X^1\Sigma_g{}^+,\ v > 4)$, $N_2(X^1\Sigma_g{}^+,\ v > 13)$, and $N_2(X^1\Sigma_g{}^+,\ v > 18)$ densities present a significant increase in the residence time interval between ∼1 and ∼15 ms. As reactants of reactions D10, D9 and D11, this behavior corroborates the fast increase in dissociation rates. Moreover, the electronically excited states' densities also present a significant increase in this time interval producing a synergy effect in the dissociation rates. As will be evidenced in figure 6, the fast increase of the species densities resulting in the fast increase of dissociation rates, and finally of the $N(^4S)$ density, results from the $N_2(X^1\Sigma^+{}_g)$ VDF heating with the discharge gas residence time. It is observed that the VDF heats considerably with the residence time; from 1 to 15 ms. At 15 ms, it undergoes its maximum excitation, and after that, there is a decrease of excitation of the VDF (see the curve at 100 ms). This VDF behavior explains the vibrational states density abrupt increase and the electronically excited states, which are also formed by reactions that depend on the vibrational states (see reactions in [21]). Under the condition of strong vibrational excitation the main excitation channels for the metastable molecules $N_2(A^3\Sigma^+{}_u)$ and $N_2(a'^1\Sigma^-{}_u)$ are reactions:

$$2 \times N_2(X^1\Sigma_g{}^+,\ v > 11) \rightarrow N_2(A^3\Sigma^+{}_u) + N_2(X^1\Sigma_g{}^+, v) \text{ and} \quad (4)$$

$$2 \times N_2\left(X^1\sum_g{}^+, v > 15\right) \rightarrow N_2\left(a'\sum_u{}^-\right) + N_2\left(X^1\sum_g{}^+, v\right). \quad (5)$$

The rate constant of reaction (4) is assumed as 10^{-17} cm^3 s^{-1} as proposed in the work of Loureiro *et al* [42]. This rate constant was obtained from the principle of detailed balance under consideration of $N_2(A^3\Sigma^+{}_u)$ quenching by the $N_2(X^1\Sigma_g{}^+, v = 0)$ molecules reaction rate constant. The low value for the rate constant of reaction (4) should be expected since this reaction is forbidden by spin conservation rules. The rate constant of reaction (5) was obtained from the work of Gordiets *et al* [41], its value is scaled as a function of the gas temperature ($k = 2.1 \times 10^{-14}\ e^{\frac{-700}{T}}$ cm^3 s^{-1}) and is 4.7×10^{-15} cm^3 s^{-1} for our measured gas temperature of

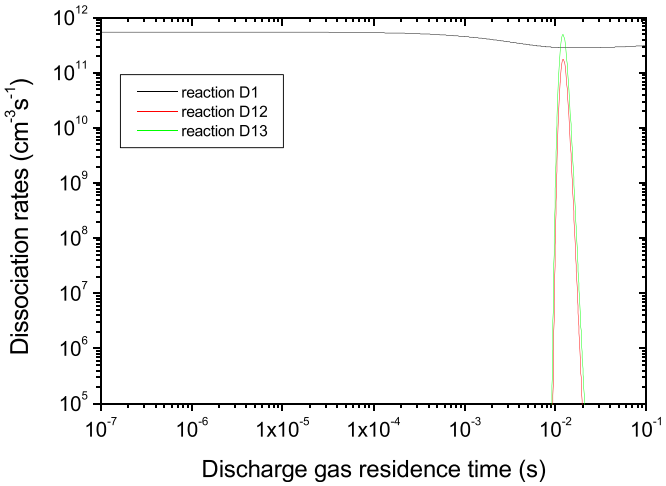

Figure 7. Dissociation rates from electron collisions with molecules in the ground state (reaction D1), and dissociation rates from pure vibrational mechanisms (reactions D12 and D13). The curves are specified in the figure legend.

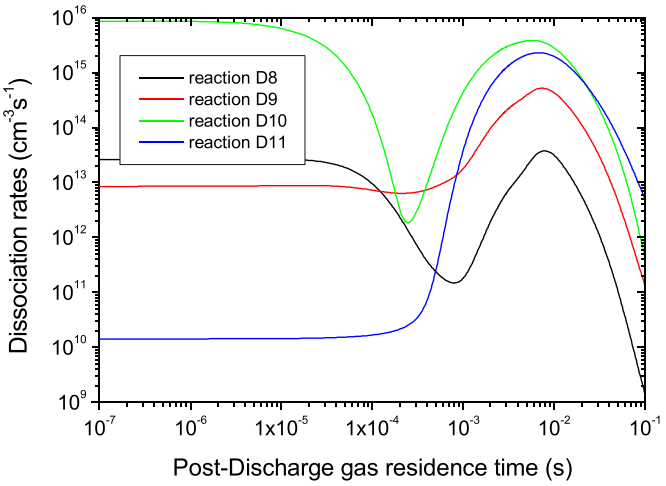

Figure 8. Dissociation rates of excited molecule collisions processes in the post-discharge (reactions D8–D11 in table 2). The curves representing the dissociation rates for each specific reaction are defined in the figure legend.

470 K. Levaton *et al* scaled this rate constant as a function of temperature based on the agreement of their measured and calculated electric field in a wide range of discharge current and gas pressure values of the studied DC discharge. Reaction (5) plays an important role in the estimation of the electric field in their work. It has been shown that reaction (5) plays an important role in the ionization processes of the pink afterglow [5, 23] in the flowing nitrogen DC discharge. We evidence the important role of the $N_2(X^1\Sigma^+_g)$ VDF of the positive column in its dissociation mechanisms for a discharge operating at a low value of the reduced electric field (see table 1).

In order to complete our analysis of the dissociation mechanisms in the positive column, we present in figure 7 the dissociation rates of the vibrational–vibrational (V–V), and inverse vibrational–translational (V–T) dissociation mechanisms, or reactions D12–D13. These are the PVM of the discharge [9]. It is observed that the PVM shows a localized contribution in dissociation rates being significant with respect to the electron collision dissociation mechanism (reaction D1) only at residence times of ∼10 ms. The contribution of these mechanisms is not important compared to the collisional dissociation mechanisms of excited molecules (see figure 4). This can be understood since the PVM dissociation reactions depend on the density of the 45th vibrational level of the $N_2(X^1\Sigma^+_g, v)$ molecules (see reactions D12 and D13 in table 2), which does not reach high values as can be seen in figure 6.

As we have analyzed the dissociation rates in the positive column, we will study the dissociation mechanisms in the nitrogen post-discharge. We observed in figure 2 the behavior of the $N(^4S)$ atoms density in the post-discharge. It follows the typical behavior of nitrogen species in the pink afterglow, that is, an increase to a maximum density and after a decrease at times ranging from ∼1 to ∼100 ms [14, 19]. In figure 8, we present the dissociation rates of reactions D8–D11 as functions of the post-discharge residence time. The contribution of reactions D12 and D13 from the V–V and inverse V–T processes are too low and will be not presented here. We should point out that the D1–D7 reactions, which are the collisions of the electron dissociation mechanisms, are not considered due to the low electron temperature in the post-discharge [5].

We can observe that the D10 and D11 reactions are the dominant dissociation mechanisms at typical times for the occurrence of the pink afterglow, which happens between ∼1 and ∼80 ms (see the experimental points in figure 2). The order of importance of the dissociation mechanisms at this time interval is the following: reactions D10, D11, D9, and D8. We have found the same importance order for dissociation mechanisms in a collision with excited molecules in the positive column at times longer than ∼4 ms (see figure 4). As a very important result, we verify that dissociation rates of reactions D10 and D11 are on the order of 2–4 $\times$ 10^{15} cm^{-3} s^{-1} at the maximum of the pink afterglow (see the curves for reactions D10 and D11 at $t \sim$ 5–7 ms in figure 8). These values are close to the maximum dissociation rates reached in the positive column, which are on the order of 10^{16} cm^{-3} s^{-1} (see curve of reaction D10 at $t \sim$ 15 ms in figure 4). This fact evidences the effectiveness of dissociation mechanisms in the post-discharge. The same behavior has been found for the ionization rates of the pink afterglow as compared to ionization rates reached in the positive column [20]. The dissociation rates of the D10 reaction are very strong in the early post-discharge residence times, reflecting the high density of nitrogen-excited species early in the post-discharge. We should remember that these initial densities correspond to the densities of nitrogen species at the end of the positive column. Also, the dissociation rate profiles in the post-discharge present the typical behavior of the excited species density profiles in the pink afterglow. These last features of the dissociation rate profiles

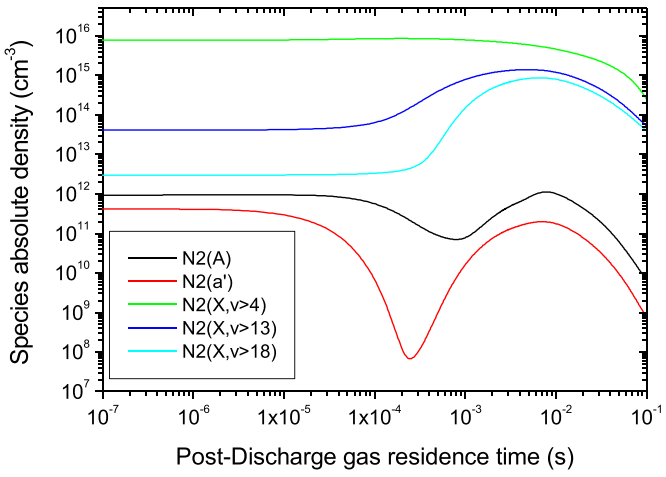

Figure 9. The absolute densities of electronically excited states and $N_2(X^1\Sigma^+_g)$ vibrational states in the post-discharge.

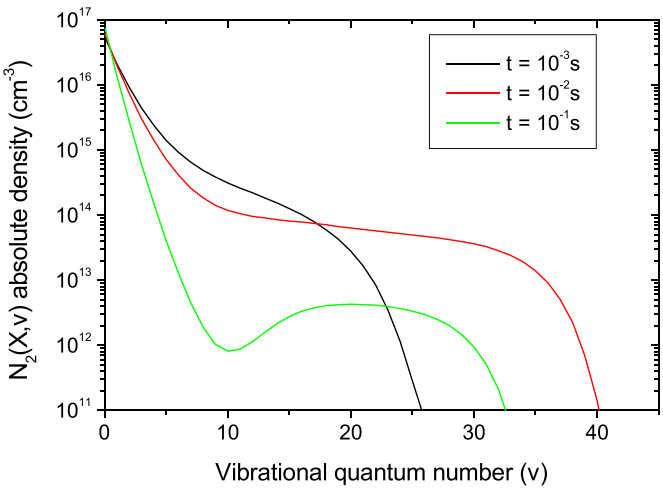

Figure 10. The $N_2(X^1\Sigma^+_g)$ VDF in the post-discharge for post-discharge residence times of 1, 10, and 100 ms.

can be well understood if we analyze the density profiles of reactants of reactions D8–D11 in the post-discharge. Figure 9, shows the reactants density profiles of reactions D8–D11 in the post-discharge. The densities of electronically excited states follow the typical behavior of nitrogen-excited species in the pink afterglow [5, 14, 19], with the maximum densities after the initial decreasing part of the curves occurring at residence times of ∼8 ms. The densities of excited vibrational states also exhibit similar behavior with their maximum densities occurring at different residence times, these times being longer as we consider higher vibrational states.

In a general way the residence times corresponding to reactants maximum densities (see figure 9) approach the residence times corresponding to the maximum values of the dissociation rates in the pink afterglow. As we have found in the positive column (see figures 4 and 5), the dissociation rate profiles follow the combined behavior of the reactants density profiles in the post-discharge. The local dissociation phenomenon in the post-discharge (see the calculated and experimental N(^{4}S) density in figure 2) is explained by the local production of the reactants of the dissociation mechanisms in the pink afterglow. As occurred in the positive column, the local increase in post-discharge dissociation rates results from the $N_2(X^1\Sigma^+_g)$ VDF relaxation with the post-discharge residence time. It should be remembered that the reactants of the dominant dissociation mechanisms (reactions D10 and D11) are the vibrational states, and the $N_2(a'^1\Sigma^-_u)$ state, which also depends on the vibrational states as reactants in the post-discharge [5, 22]. Figure 10 presents the $N_2(X^1\Sigma^+_g)$ VDF evolution with the post-discharge residence time for our experimental condition. We can observe the heating of the VDF from 1 to 10 ms residence times. After its maximum excitation at 10 ms, the VDF is depopulated. This VDF behavior resulting from the V–V and V–T exchange reactions [5] explains the behavior of the reactants of the dissociation mechanisms, and finally of the N(^{4}S) density profile in the pink afterglow. At this point, it is evidenced the very important role of the $N_2(X^1\Sigma^+_g)$ VDFs in the dissociation mechanisms occurring in the pink afterglow plasma, and equally in the positive column of a flowing nitrogen DC discharge operating at a low value of the reduced electric field (see table 1).

Having studied the dissociation mechanisms of the positive column and pink afterglow plasmas, we will now analyze their atoms' excitation mechanisms. Here, we will study the N(^{2}D) and N(^{2}P) excitation mechanisms. We consider these mechanisms between the 115 physical-chemical reactions of the positive column [21] and 66 physical-chemical mechanisms for the post-discharge [22]. The excitation mechanisms of the N(^{2}D) atoms are listed in table 3. The excitation mechanisms of the N(^{2}P) atoms are listed in table 4. We should point out that the E1, E2 and F1 reactions are neglected in the post-discharge due to its low mean electron energy [5]. The excitation rates are defined as the product of the reactants concentrations and rate constant of reactions E1–E5 and F1–F3 of tables 3 and 4, respectively.

We calculated the rates for the excitation of N(^{2}D) and N(^{2}P) atoms in the positive column. Figure 11 shows the excitation rates for the reactions E1–E5 concerning the excitation of the N(^{2}D) atoms. We can observe that electron collisions with the ground state molecules $N_2(X^1\Sigma_g{}^+)$ dissociative mechanism (reaction E2) is the dominant N(^{2}D) excitation channel in the positive column from the earlier discharge residence times up to 0.6 ms. From 0.6 ms up to 3 ms, electron collisions with the N(^{4}S) atoms (reaction E1) become the dominant excitation channel for the metastable atoms. After 3 ms, we observe that reaction E3 becomes the dominant excitation channel for the N(^{2}D) atoms. Reaction E4 presents a localized contribution to the excitation rates at times on the order of 10 ms. The rapid increase in the excitation rates of the E3 reaction, from ∼3 ms to ∼20 ms, explains the strong increase of the N(^{2}D) atoms density in this time interval (see red line in figure 1). Reaction E3 was proposed in [44] to explain the local increase of the N(^{2}D) density in the pink afterglow of flowing nitrogen DC discharges [37]. Still, its rate constant presents a relatively low

Table 3. Physical-chemical mechanisms leading to $N(^2D)$ excitation in the positive column and post-discharge.

Process: $N(^2D)$ excitation mechanisms		k ($cm^3 s^{-1}$)	References
E1	$e + N(^4S) \rightarrow e + N(^2D)$	$f(T_e)$	[43]
E2	$e + N_2(X^1\Sigma_g^+) \rightarrow e + N(^4S) + N(^2D)$	$f\left(\frac{E}{N}, T_g, n_e, p\right)$	[35]
E3	$N_2(X^1\Sigma_g^+, v > 8) + N(^4S) \rightarrow N(^2D) + N_2(X^1\Sigma_g^+, v = 0)$	7×10^{-14}	[44]
E4	$N_2(X^1\Sigma_g^+, v > 38) + N(^4S) \rightarrow N(^2D) + N_2(A^3\Sigma^+_u)$	10^{-11}	[45]
E5	$N(^2P) + N(^4S) \rightarrow N(^2D) + N(^4S)$	1.8×10^{-12}	[32]

Table 4. Physical-chemical mechanisms leading to $N(^2P)$ excitation in the positive column and post-discharge.

Process: $N(^2P)$ excitation mechanisms		k ($cm^3 s^{-1}$)	References
F1	$e + N(^4S) \rightarrow e + N(^2P)$	$f(T_e)$	[43]
F2	$N_2(X^1\Sigma_g^+, v > 13) + N(^4S) \rightarrow N(^2P) + N_2(X^1\Sigma_g^+, v = 0)$	10^{-14}	[22]
F3	$N_2(A^3\Sigma^+_u) + N(^4S) \rightarrow N(^2P) + N_2(X^1\Sigma_g^+, v = 0)$	4×10^{-11}	[46]

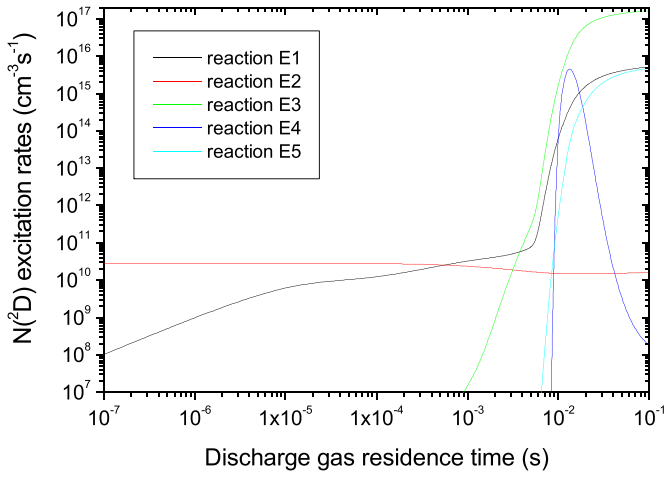

Figure 11. Excitation rates for the $N(^2D)$ atoms as functions of the discharge gas residence time. The reactions are specified in the figure legend (see reactions in table 3).

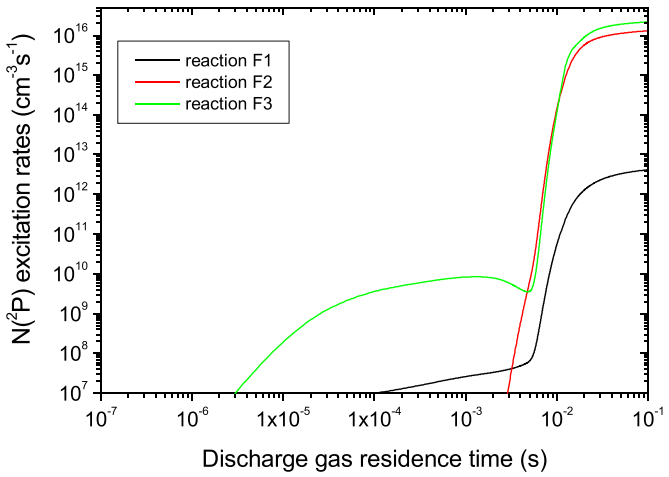

Figure 12. Excitation rates for the $N(^2P)$ atoms as functions of the discharge gas residence time. The reactions are specified in the figure legend (see reactions in table 4).

value (see table 3), the densities of its reactants, $N(^4S)$ atoms (see black line in figure 1) and $N_2(X^1\Sigma_g^+, v > 8)$ states (see the curves for the $N_2(X^1\Sigma_g^+, v > 4)$ and $N_2(X^1\Sigma_g^+, v > 13)$ states as reference in figure 5), reach considerable values at times of ∼10 ms. As we have observed here in the dissociation mechanisms of the positive column and pink afterglow, the $N_2(X^1\Sigma_g^+, v)$ states also play an important role in the excitation of the $N(^2D)$ atoms. Therefore, we have evidenced that the VDF behavior in the positive column strongly affects the dissociation and $N(^2D)$ excitation mechanisms.

Let us now analyze the $N(^2P)$ atoms excitation mechanisms in the positive column. Figure 12 shows the excitation rates of reactions F1–F3 (see table 4), concerning the excitation of $N(^2P)$ atoms. We can observe that electron collisions with the ground state atoms $N(^4S)$ excitation mechanism (reaction F1) play a minor role in the studied range of residence times in the positive column. Reaction F3 dominates the excitation of the $N(^2P)$ atoms at discharge residence times inferior to ∼4 ms. After 4 ms, reactions F2 and F3 present almost the same contribution in the excitation rates. Both present an abrupt increase from times of ∼4 ms up to ∼20 ms explaining the strong increase in the density of $N(^2P)$ atoms (see green line in figure 1). The fact that the excitation of $N(^2P)$ atoms presents a low dependence on the electrons collisions mechanism (reaction F1) can be understood as a result of the low value of the reduced electric field studied here (see table 1).

As a final point, the $N(^2D)$ and $N(^2P)$ excitation mechanisms were studied in the post-discharge. We calculated the rates of their excitation mechanisms as functions of the post-discharge gas residence time. Figure 13 shows the excitation rates of reactions E3–E5 (see table 3) in the nitrogen post-discharge. We can observe that reaction E3 is the dominant $N(^2D)$ excitation mechanism in the entire range of post-discharge residence times analyzed. The rates of such a mechanism reach values of the order of 10^{16} cm^{-3} s^{-1} at the maximum excitation occurring at residence times of ∼10 ms in the post-discharge. These values are significant if we consider the same excitation rates in the positive column (see the red line at $t \sim 10$ ms, in figure 11). This fact demonstrates the high effectiveness of local excitation of $N(^2D)$ atoms in the

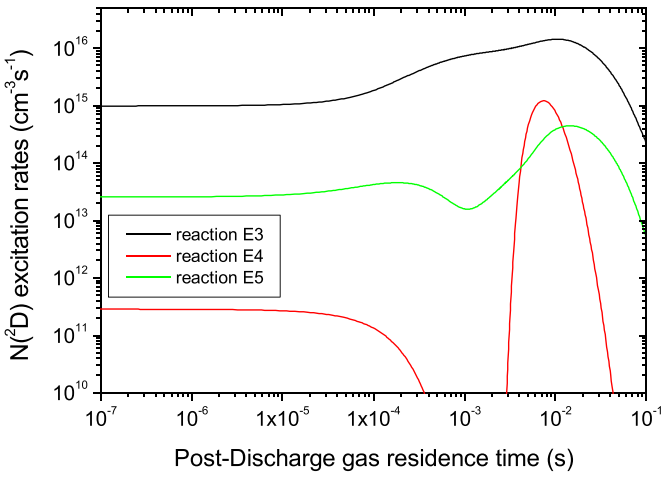

Figure 13. N(^{2}D) excitation rates in the post-discharge (reactions E3–E5 in table 3). The curves representing the excitation rates for each specific reaction are defined in the figure legend.

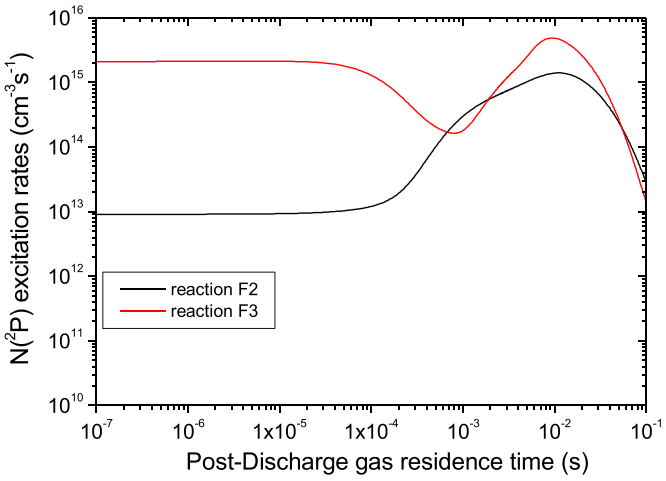

Figure 14. N(^{2}P) excitation rates in the post-discharge (reactions F2–F3 in table 4). The curves representing the excitation rates for each specific reaction are defined in the figure legend.

pink afterglow. Reaction E4 presents a low contribution to the excitation rates only at times of the order of ∼6 ms. We can also verify that the N(^{2}D) density profile (see figure 2) follows the trend of the excitation rates of reaction E3. We verify that reaction E3 plays a dominant role in the positive column at times longer than ∼3 ms (see figure 11), and also in the nitrogen post-discharge. Since one of the reactants of this excitation mechanism are the vibrational states (see table 3), we find a strong dependence of N(^{2}D) excitation on the VDFs heating occurring in the discharge and post-discharge (see figures 6 and 10).

The excitation rates of the N(^{2}P) atoms in the post-discharge are shown in figure 14. We find that the N(^{2}P) excitation rates of reaction F3, proposed by Piper [46], are dominant from the earlier post-discharge residence times up to ∼0.5 ms. After 0.5 ms, reactions F2 and F3 alternate the dominant role of the N(^{2}P) atoms excitation with the residence time in the post-discharge. We observe that the maximum excitation rate value reached by reaction F3 is $\sim 5 \times 10^{15}$ cm^{-3} s^{-1} at $t \sim 10$ ms. This is a significant rate value if we compare the role of the N(^{2}P) excitation mechanisms in the positive column (see rates of reactions F2 and F3 at discharge residence times of ∼10 ms, in figure 12). Therefore, as we have observed for the N(^{2}D) atoms, we also found an effective local excitation of N(^{2}P) atoms in the pink afterglow.

4. Conclusion

In this work, we studied the molecular dissociation and the N(^{2}D) and N(^{2}P) atoms excitation mechanisms occurring in the positive column and pink afterglow plasma of a flowing nitrogen DC discharge operating at 30 mA discharge current, 0.5 Slm^{-1} gas flow rate, and 500 Pa gas pressure. The discharge has characteristics of the experimental parameters an electron density (n_e) of $(5.66 \pm 0.15) \times 10^{10}$ cm^{-3} and a reduced electric field (E/N) of 25 ± 3 Td (see table 1, for the complete set of experimental parameters). These experimental conditions have allowed the detection of the pink afterglow plasma in the post-discharge tube (see section 2). We constructed two kinetic numerical models, one for the positive column, and the other for the pink afterglow, that were utilized in the calculations of the temporal dissociation and atoms excitation rates of these two different nitrogen plasmas. We computed 13 different dissociation mechanisms and 8 atoms excitation mechanisms with the kinetic numerical models for our experimental condition. Our study permitted the detailed analysis of a set of dissociation and atomic excitation mechanisms for the experimental condition analyzed. We should take into account that our observations concern only a unique discharge condition where the reduced electric field presents a low value of 25 Td. Moreover, we studied the electron collision dissociation mechanisms considering only the fundamental vibrational level of the nitrogen molecules. The electron collision dissociation mechanisms involving higher vibrational levels of the nitrogen molecules in the electronic fundamental state are not considered here. Work is in progress to unveil the dissociation and atomic excitation mechanisms for a wider set of reduced electric field values and with consideration of the vibrational manifold of the $N_2(X^1\Sigma_g^+)$ molecules in the electron collision dissociation mechanism. Taking into account the limitations of our analysis we have observed the following kinetics characteristics concerning dissociation and atomic excitation resulting from the present analysis. Concerning the dissociation mechanisms, we observed that reaction $e + N_2(X^1\Sigma_g^+, v = 0) \rightarrow e + N(^4S) + N(^4S)$ is the main dissociation channel in the positive column from the earlier discharge residence times up to ∼2 ms. From 2 ms up to 0.1 s, the collisions between excited molecules become the main dissociation mechanisms. In between these collisional processes, the most efficient dissociation mechanisms are the reactions $N_2(a'^1\Sigma^-_u) + N_2(X^1\Sigma_g^+, v > 4) \rightarrow N(^4S) + N(^4S) + N_2(X^1\Sigma_g^+, v)$ and $2 \times N_2(X^1\Sigma_g^+, v > 18) \rightarrow N(^4S) + N(^4S) + N_2(X^1\Sigma_g^+, v)$. We observed in the

pink afterglow that these last reactions are also the dominant dissociation channels in the post-discharge. The dissociation rates found in the maximum of the pink afterglow are significant as compared to the dissociation rates found in the positive column. This result evidences the effectiveness of dissociation mechanisms occurring in the nitrogen pink afterglow. We analyzed the $N_2(X^1\Sigma_g{}^+, v)$ VDFs in the positive column and pink afterglow. Our results demonstrate that the dissociation mechanisms of the positive column and pink afterglow are strongly dependent on the VDFs behavior in the discharge and post-discharge. We also analyzed the $N(^2D)$ and $N(^2P)$ excitation mechanisms. We found in the positive column, for times below 0.6 ms, that reaction $e + N_2(X^1\Sigma_g{}^+) \rightarrow e + N(^4S) + N(^2D)$ is the main excitation mechanism of the $N(^2D)$ atoms. At the time interval from 0.6 ms up to 3 ms, reaction $e + N(^4S) \rightarrow e + N(^2D)$ is the main $N(^2D)$ excitation channel. For longer discharge residence times the reaction $N_2(X^1\Sigma_g{}^+, v > 8) + N(^4S) \rightarrow N(^2D) + N_2(X^1\Sigma_g{}^+, v)$ becomes the dominant excitation channel of the $N(^2D)$ atoms. We verified that the last reaction is also the dominant excitation mechanism in the pink afterglow. In this sense, we found that the $N(^2D)$ atoms excitation mechanisms of the positive column and pink afterglow plasma depend strongly on the VDFs of the discharge and post-discharge. The important role of the VDFs in the discharge and post-discharge may be understood as a consequence of the low value of the reduced electric field ($E/N = 25$ Td) studied in the positive column. The EEDF for this value of E/N is not too excited, and this fact brings as results the low efficiency of electrons collisional processes. In the post-discharge, or in the pink afterglow, electrons collisional processes are not considered due to the low electron temperature of the post-discharge. Finally, we observed that the most efficient $N(^2P)$ atoms excitation mechanism in the positive column and pink afterglow is the reaction $N_2(A^3\Sigma^+{}_u) + N(^4S) \rightarrow N(^2P) + N_2(X^1\Sigma_g{}^+, v)$. However, the reaction $N_2(X^1\Sigma_g{}^+, v > 13) + N(^4S) \rightarrow N(^2P) + N_2(X^1\Sigma_g{}^+, v)$ presents a significant contribution to the excitation rates at certain discharge and post-discharge residence times. Our work brings for the first time a temporal analysis of the dissociation and atoms excitation mechanisms in two different nitrogen plasmas, the positive column, and the pink afterglow.

Data availability statement

The data that support the findings of this study are available upon reasonable request from the authors.

Acknowledgments

J Levaton would like to thank CNPq—Brazil for the Grant No. 101877/2022-6.

ORCID iDs

J Levaton https://orcid.org/0000-0003-1136-1971
J Amorim https://orcid.org/0000-0002-9250-4681
J H F Severo https://orcid.org/0000-0001-6271-666X

References

[1] Ricard A, Oseguera-Pena J E, Falk L, Michel H and Gantois M 1990 *IEEE Trans. Plasma Sci.* **18** 940
[2] Malvos H, Michel H and Ricard A 1994 *J. Phys. D: Appl. Phys.* **27** 1328
[3] Capitelli M 1986 *Topics in Current Physics: Nonequilibrium Vibrational Kinetics* (Berlin: Springer)
[4] Armenise I, Capitelli M, Garcia E, Gorse C, Lagana A and Longo S 1992 *Chem. Phys. Lett.* **200** 597–604
[5] Levaton J, Amorim J, Souza A R, Franco D and Ricard A 2002 *J. Phys. D: Appl. Phys.* **35** 689
[6] Czerwiec T, Greer F and Graves D B 2005 *J. Phys. D: Appl. Phys.* **38** 4278
[7] Levaton J, Ricard A, Henriques J, Silva H R T and Amorim J 2006 *J. Phys. D: Appl. Phys.* **39** 3285
[8] Volynets A V, Lopaev D V, Rakhimova T V, Chukalovsky A A, Mankelevich Y A, Popov N A, Zotovich A I and Rakhimov A T 2018 *J. Phys. D: Appl. Phys.* **51** 364002
[9] Cacciatore M, Capitelli M and Gorse C 1982 *Chem. Phys.* **66** 141
[10] Kumar S and Ghosh P K 1991 *Chem. Phys. Lett.* **179** 463
[11] Guerra V, Galiaskarov E and Loureiro J 2003 *Chem. Phys. Lett.* **371** 576
[12] Diamy A M, Legrand J C, Moritts A and Ricard A 1999 *Surf. Coat. Technol.* **112** 38
[13] Levaton J, Amorim J and Franco D 2005 *J. Phys. D: Appl. Phys.* **38** 2204
[14] Levaton J, Amorim J and Ricard A 2012 *J. Phys. D: Appl. Phys.* **45** 505203
[15] Krcma F and Záková M 2009 *Eur. Phys. J.* D **54** 369
[16] Krcma F, Mazánková V and Soural I 2006 *Czech. J. Phys.* **56** B871
[17] Bromer H H and Hesse J 1969 *Z. Phys.* **219** 269
[18] Beale G E and Broida H P 1959 *J. Chem. Phys.* **31** 1030
[19] Sadeghi N, Foissac C and Supiot P 2001 *J. Phys. D: Appl. Phys.* **34** 1779
[20] Levaton J, Klein A N, Amorim J and Severo J H F 2021 *J. Appl. Phys.* **54** 505205
[21] Levaton J, Klein A N and Amorim J 2020 *Phys. Plasmas* **27** 063503
[22] Levaton J and Amorim J 2014 *Chem. Phys.* **435** 1
[23] Levaton J, Klein A N and Binder C 2018 *Plasma Chem. Plasma Process.* **38** 1259
[24] Lofthus A and Krupenie P H 1977 *J. Phys. Chem. Ref. Data* **6** 113
[25] Levaton J, Amorim J, Monna V, Nagai J and Ricard A 2004 *Eur. Phys. J. Appl. Phys.* **26** 59
[26] Hochard L, Magne L, Cernogora G and Peeters J 1994 *12th ESCAMPIG* (*Noordwijkerhout, Netherlands*) vol 18E p 336
[27] Press W H, Flannery B P and Vetterling W T 1992 *Numerical Recipes in C: The Art of Scientific Computing* (Cambridge: Cambridge University Press)
[28] Shampine L F and Reichelt M R 1997 *SIAM J. Sci. Comput.* **18** 1
[29] Levaton J, Klein A N and Amorim J 2021 *Braz. J. Phys.* **51** 75
[30] Levaton J, Klein A N, Amorim J and Binder C 2019 *Plasma Res. Express* **1** 045004
[31] Popov N A 2009 *Plasma Phys. Rep.* **35** 436
[32] Matveyev A A and Silakov V P 1999 *Plasma Sources Sci. Technol.* **8** 162
[33] Salmon A, Popov N, Stancu G and Laux C 2018 *J. Phys. D: Appl. Phys.* **51** 314001
[34] Lin C L and Kaufman F 1971 *J. Chem. Phys.* **55** 3760
[35] Cosby P C 1993 *J. Chem. Phys.* **98** 9544
[36] Bockel S, Diamy A M and Ricard A 1995 *Surf. Coat. Technol.* **74** 474
[37] Amorim J and Kiohara V 2004 *Chem. Phys. Lett.* **385** 268

[38] Eslami E and Sadeghi N 2008 *Eur. Phys. J. Appl. Phys.* **43** 93
[39] Itikawa Y 2006 *J. Phys. Chem. Ref. Data* **35** 31
[40] Bacri J and Medani A 1982 *Physica* B+C **112** 101
[41] Gordiets B, Ferreira C M, Pinheiro M J and Ricard A 1998 *Plasma Sources Sci. Technol.* **7** 363
[42] Loureiro J, Sá P A and Guerra V 2001 *J. Phys. D: Appl. Phys.* **34** 1769
[43] Huo W M, Liu Y, Panesi M, Munafo A, Wray A and Carbon D F 2015 *Electron-Impact Excitation Cross Sections for Modeling Non-Equilibrium Gas* (available at: https://ntrs.nasa.gov/search.jsp?R=20160000198)
[44] Levaton J and Amorim J 2012 *Chem. Phys.* **397** 9
[45] Sá A, Guerra V, Loureiro J and Sadeghi N 2004 *J. Phys. D: Appl. Phys.* **37** 221
[46] Piper L G 1989 *J. Chem. Phys.* **90** 7087